



STScI | SPACE TELESCOPE
SCIENCE INSTITUTE

Instrument Science Report ACS 2021-01

Systematic Effects of Pixel-based CTE Correction on the Accuracy of ACS/WFC Point Source Polarimetry

T. D. Desjardins, D. D. Carter, D. C. Hines, N. D. Miles, A. Bellini

April 29, 2021

ABSTRACT

We present a study of simulated ACS/WFC observations to assess the accuracy of point source polarimetry after application of the pixel-based CTE correction. We find evidence of a small offset between the measured and intrinsic polarization fraction ($P - P_0 \leq 0.01$) in the CTE-corrected data that is positively correlated with polarization fraction and the number of y -transfers to reach the serial register. No strong correlation is observed between the polarization fraction offset and other parameters in the non-CTE-corrected data. Conversely, we find that the Stokes parameters measured from the CTE-corrected data are better recovered compared to the non-CTE-corrected data, which exhibit a relatively large offset across the WFC CCDs. These results serve as a first step in the analysis of the effects due to the pixel-based CTE correction on correlated, derived values of scientific interest such as polarimetry measurements.

1 Introduction

The Advanced Camera for Surveys (ACS) Wide Field Channel (WFC) and High Resolution Channel (HRC) detectors use a common set of two filter wheels each containing three polarizing filters mounted at 60° rotations with respect to each other. On Filter Wheel 1, the polarizers are optimized for blue and near-UV observations (POLUV), while the polarizing

filters on Filter Wheel 2 are optimized for blue to red visible light (POLV). With this configuration, ACS is capable of observing polarized light by crossing the polarizing filters with another imaging filter, e.g., the F606W filter (on Filter Wheel 1) in combination with the Filter Wheel 2 POLV filters (see the ACS Instrument Handbook section 6.1 for a list of all available and supported filter combinations; Ryon et al. 2021). Note that the ACS polarizing filters are designed to only measure linear polarization.

Continuous bombardment of the CCDs by high energy particles in the low-Earth orbit radiation environment has a degrading effect on detector performance. One of the ways this degradation manifests is via loss of charge transfer efficiency (CTE). Photons striking the CCDs are recorded as photoelectrons stored in the potential well of each pixel. During readout, some of this charge is trailed into pixels in the column-wise direction toward the serial register due to an increasing population of charge traps created by the aforementioned degradation of the CCDs. If the displacement of photoelectrons due to CTE loss is large enough, some photoelectrons may be displaced out of a photometric aperture and decrease the measured fluence of a source. The magnitude of this charge displacement is dependent upon the number of transfers the charge undergoes in the column-wise (y) direction to arrive at the serial register, the brightness of the source, and the sky background level. Furthermore, the CTE loss worsens over time due to the cumulative nature of the radiation-induced degradation of the CCDs (Riess & Mack, 2004; Ubeda et al., 2012; Ryon & Grogin, 2018).

To compensate for CTE loss, a user may correct either measured photometry (i.e., photometric CTE correction; see, e.g., Riess 2003; Riess & Mack 2004; Chiaberge et al. 2009; Chiaberge 2012) or the image before performing photometry. Anderson & Bedin (2010) introduced the pixel-based CTE correction algorithm for ACS (further refined by Anderson & Ryon 2018), which produces images wherein the pixels have been corrected for CTE loss. Testing has shown that the pixel-based CTE correction performs well for a wide range of source fluences and background levels. While demonstrated to be accurate, the photometric CTE correction is limited to correcting the photometry of point sources, and thus extended sources rely on the pixel-based correction. This has made the use of CTE-corrected images (i.e., FLC and DRC images) common for many ACS users.

In this report, we begin an investigation of the effects of CTE data processing on the accuracy of ACS polarimetry. The scope of this report is limited to the effects of the pixel-based CTE correction on polarimetry observations of point sources¹. We intend this report to serve as the basis of future studies that expand this analysis to extended sources and perhaps other types of data processing (e.g., drizzling). This report is organized as follows: in Section 2 we describe our data and analysis methods, in Section 3 we present our results, and in Section 4 we summarize our findings and discuss future work.

¹Note that CTE-corrected data are not automatically produced by the ACS data pipeline for subarray data, and thus for polarimetry observations. Users who want to analyze CTE-corrected polarimetry data must remove bias striping (for post-2009 data) and run the CTE correction algorithm. The `acs_destripe_plus` code in `acstools` can be used for this purpose. See the ACS website at <http://www.stsci.edu/hst/instrumentation/acs> for a Jupyter notebook example.

2 Data and Analysis

2.1 Simulation Parameters

For this study, we use simulations of ACS observations to assess the impact of CTE correction on measuring Stokes parameters, and thus polarization properties. To facilitate this goal, we define a grid of simulation inputs: polarization fraction (P ; 0.02, 0.05, 0.1, 0.2, 0.3, 0.5, 0.8, and 1)² and source brightness ($13 \leq m_{\text{F606W}} \leq 20$ ST magnitudes in steps of 0.5 magnitudes). These parameters yield 120 unique permutations. Note that we fix the average sky background to $20 e^-$ per pixel³, the polarization angle (θ) of our simulated stars to 45° , and the date of our simulated observations to January 1, 2020 00:00:00 UTC to account for any time-dependent effects (e.g., the CTE correction). We use `pysynphot` (STScI Development Team, 2013) to determine count rates in each of the three polarizing filters by first backing out the Stokes I , Q , and U values for a given input polarization. From the ACS Data Handbook (Lucas et al., 2021), we can express the polarization fraction P and position angle θ as a combination of the Stokes parameters as follows:

$$P = \frac{\sqrt{Q^2 + U^2}}{I}$$

and

$$\theta = \frac{1}{2} \tan^{-1} \left(\frac{U}{Q} \right) + \text{PAV3} + \chi,$$

where I , Q , and U represent the Stokes parameters, PAV3 is the position angle of the V3 axis of the telescope, and χ is a detector-dependent constant to correct for the mounting position of the detector in the optical path (for WFC, $\chi = -38.2^\circ$). For this study, we choose PAV3 to be equal to 38.2° such that it cancels out the χ term for simplicity. This combination of θ and χ results in all of the polarization power being in the Stokes U parameter, while Stokes Q is effectively zero.

The Stokes parameters can be expressed as a combination of photometric measurements:

$$I = \frac{2}{3} (r_0 + r_{60} + r_{120}),$$

$$Q = \frac{2}{3} (2r_0 - r_{60} - r_{120}),$$

and

$$U = \frac{2}{\sqrt{3}} (r_{60} - r_{120}),$$

where the r_N terms represent a photometric measurement in the polarizing filter rotated at angle N (e.g., r_{120} represents POL120V or POL120UV depending on the filter set in use). By

²We did examine the $P = 0$ case as well; however, we found that, due to the Rician distribution of the polarization fraction, we obtained much larger offsets ($\Delta P \approx 0.05$) between the polarization measured from the simulated data and the intrinsic polarization compared to simulations of even small fractions of polarization. Despite this, these offsets are statistically consistent with no effect.

³This is the minimum recommended sky background level for ACS/WFC observations to mitigate the effects of CTE loss. See the Advice for Planning ACS Observations page at <https://hst-docs.stsci.edu/acsoam> for more information.

combining the above equations, we can calculate the count rate in each polarizing filter for an input source magnitude m_{F606W} , polarization fraction P , and $\theta = 45^\circ$. Though we have specified our input source magnitudes in the F606W filter, the filter choice does not affect our method or results⁴, but only serves to limit our source brightness to a range suitable for ACS polarimetry.

A source with little or no polarization will produce a roughly equal count rate in each of the three polarizing filters, while increasing polarization fractions will produce a more unequal distribution of count rates. It is therefore common for observers to adjust exposure times in each filter to increase the signal-to-noise (S/N) of each observation, and to use the source count rates (rather than source counts) in the equations above. To account for the difference in total counts (and thus the Poisson noise) between the polarizing filters, we selected exposure times for our simulated images to achieve a fixed S/N = 260 in each polarizing filter. This S/N value follows from the polarization uncertainty published by Sparks & Axon (1999), which states that

$$\log_{10} \left(\frac{\sigma_P}{P} \right) = -0.102 - 0.9898 \log_{10} (P \langle \text{S/N} \rangle_i),$$

where $\langle \text{S/N} \rangle_i$ is the average S/N of the three input images. Similarly, the accuracy of the polarization position angle θ is given by Sparks & Axon (1999) as

$$\log_{10} (\sigma_\theta) = 1.415 - 1.068 \log_{10} (P \langle \text{S/N} \rangle_i).$$

Thus, our requirement that S/N = 260 yields an accuracy of $\sigma_P \approx 0.005$ for all polarization fractions, and $0.069 \leq \sigma_\theta \leq 4.5^\circ$ for $P = 1.0$ and 0.02 (the limits of the simulation grid), respectively.

2.2 Simulating ACS/WFC Images

The ACS/WFC image simulation code⁵ (developed by Andrea Bellini and Nathan Miles) is designed to simulate full-frame ACS/WFC images, i.e., two 2048 rows \times 4096 columns CCDs that are each read out by two amplifiers using a split-serial method (see Ryon et al. 2021 for more information). Due to the vignetted field of view of the polarizing filters when coupled with the ACS/WFC, polarization data are observed as a 2048 row \times 2048 column subarray read out using amplifier B on the WFC1 CCD. The image simulation code is designed to simulate full-frame WFC images, and so rather than limit our analysis to only the subarray region used by real ACS/WFC polarization observations, we use the full-frame data to increase our sample of point sources in our simulation grid. The image simulation code places point sources in an equally-spaced grid⁶ of 3,941 total positions across both CCDs. Every other row of point sources is offset by half of the grid spacing in the x -direction to prevent CTE-trails in the y -direction overlapping with nearby point sources (see Figure 1).

⁴There are filter-dependent corrections that must be made when measuring ACS polarimetry (see the ACS Data Handbook; Lucas et al. 2021), but by simulating sources starting with input polarization properties these terms cancel out in our analysis.

⁵At the time of writing, this code has not been publicly released by its creators.

⁶The image simulation code can also be used to place point sources at specific positions, however the regularly-spaced grid was designed specifically to study CTE effects.

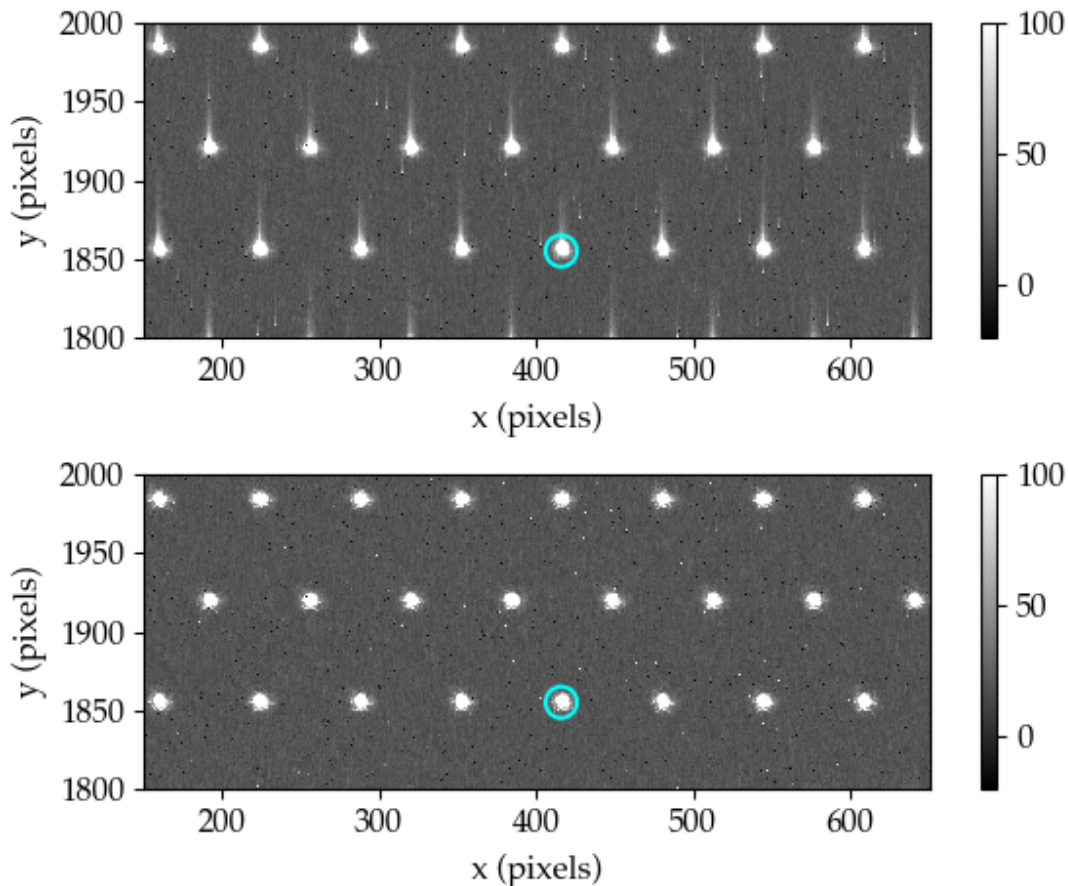


Figure 1: Simulated observations of a $m_{F606W} = 15$ ST magnitude, low-polarization ($P = 0.02$) point source with $20 e^-$ of sky background in the POL0V filter. This subset of the data is taken from a $200 \text{ row} \times 500 \text{ column}$ region of the WFC2 CCD, and shows point sources that undergo the most y -transfers to arrive at the serial register, i.e., sources that experience the worst CTE loss. In both panels, the cyan circle shows the $r = 10$ pixel aperture used for photometry for a representative point source. At this scale, detector artifacts such as sink pixels and residuals from dark current subtraction are clearly visible. (*Top*) The non-CTE-corrected “FLT” image. (*Bottom*) The CTE-corrected “FLC” image.

The placement of point sources in rows yields a sample of multiple realizations of a point source at a fixed number of y -transfers from the serial register to study the effect of the CTE correction.

The ACS simulation code begins by creating CTE-corrected effective point spread functions (ePSFs) for each location of a point source on the WFC CCDs using a PSF library based on Bellini et al. (2018). The code then includes sky background (with Poisson noise) and dark current using calibration reference files taken from the Calibration Reference Data System (CRDS). Point sources are added to the image by scaling each PSF by a number selected from a Poisson distribution with a mean equal to the input source counts. The image is then multiplied by the pixel-to-pixel flat-field. Next, the effect of CTE-loss is simulated using the ACS CTE forward model⁷, which creates an intermediate pipeline product called

⁷At the time of writing, an example Python Jupyter notebook written by Jenna Ryon that discusses

a “BLV_TMP” (hereafter BLV) file. The BLV file is corrected for CTE loss using the ACS pixel-based CTE code `acscte` to create a “BLC_TMP” (hereafter BLC) file, which is the CTE-corrected version of the BLV file in the ACS pipeline. For both the BLC and BLV files, the `acs2d` algorithm from the ACS data calibration pipeline is run to remove the dark current and divide by the flat-field. This turns both the BLC and BLV files into “FLC” and “FLT” calibrated images, respectively. We repeat this for each of the POL0V, POL60V, and POL120V polarizers at each of the 120 permutations of the grid parameters, yielding 360 each of FLT and FLC images, and 1,418,760 polarization measurements with and without CTE correction.

The image simulation code properly handles location-dependent properties of a given simulated point source, such as dark current and PSF shape, to better simulate real ACS/WFC observations. As mentioned above, we use complete full-frame simulated images rather than limit our analysis to point sources simulated in the amplifier B region associated with real polarization observations. However, the variation in simulated source properties between readout amplifiers, which we describe next, likely has a negligible impact on our results.

In January 2020 (the date used in our simulated data), the median dark current of each readout amplifier of the WFC CCDs ranged between approximately 0.011 and 0.015 $e^-/s/\text{pixel}$ (M. C. McDonald, private communication). At the lowest exposure time in our data (33 seconds), the median dark current in different readout amplifier regions results in a variance of $112 < \sigma^2 < 159 e^{-2}$ ($\Delta_{\sigma^2} = 47 e^{-2}$) integrated over the source aperture ($r = 10$ pixels), while at the longest exposure time (451 seconds) the mean dark current variance is $1530 < \sigma^2 < 2169 e^{-2}$ ($\Delta_{\sigma^2} = 639 e^{-2}$). In all cases, the simulated point sources contain 66,000 – 68,000 e^- , and thus the dark current rates likely represent a negligible contribution ($\lesssim 3\%$) to the total uncertainty compared to the Poisson noise.

The PSF varies across the WFC, and is dependent upon the filter used for the observations (see, e.g., Bellini et al. 2018). However, the simulation code does not account for the PSF effects of the polarizing filters, and only includes the F606W filter. As the goal of this study is to assess the accuracy of the polarization properties measured from CTE-corrected images, and these properties rely solely on the relative signal between the three polarizing filters, the spatial variations in the PSF across the WFC due to the F606W filter have no significant impact on our results.

2.3 Photometry

We use `photutils` (Bradley et al., 2020) to perform aperture photometry on each of our sources. The sources are placed at the same (x, y) grid location in each image, however PSF variation and noise can cause the measured centroid position of each source to shift slightly between images. To mitigate this, we select a single CTE-corrected image to serve as a positional reference for the photometric apertures used in all images (both FLC and FLT). For each point source, we use a circular aperture with radius $r = 10$ pixels to measure the source counts, and an annulus with radii $r_{\text{in}} = 15$ and $r_{\text{out}} = 20$ pixels to estimate the median local background. In the FLT images, the source aperture includes a portion of the

the CTE forward model and its use can be found in the `acs-notebook` repository at <https://github.com/spacetelescope/acs-notebook>. The code for the CTE forward model, developed by Jamie Noss and Jenna Ryon, is part of `acstools` at <https://github.com/spacetelescope/acstools>.

CTE tail. The background annulus also contains a portion of the CTE tail, however this is not a concern as the number of pixels impacted is small and we use the median of the annulus for local background subtraction. The source aperture radius that we use is larger than what is typically used for ACS photometry, which would normally increase the noise in the measurement, however our sources are all very well-detected ($S/N = 260$) and isolated by design, and therefore this is not a concern. The larger source aperture radius allows us to capture a significant portion of the CTE trail in the FLT data to compare with the FLC measurements.

3 Results

Recall from Section 2 that the expected uncertainty in our polarization measurements from Sparks & Axon (1999) is $\sigma_P \approx 0.005$ and $0.069^\circ \leq \sigma_\theta \leq 4.5^\circ$. As expected, the difference between the measured polarization fraction P and the intrinsic value P_0 for most of our data is $|P - P_0| < 3\sigma_P$. We exclude sources with values larger than this, which we consider outliers, that account for 2,332 (0.16%) and 2,378 (0.16%) of sources in the FLT and FLC data, respectively. Further investigation of these outliers shows that only ~ 100 source positions were outliers more than once, and of these approximately 50 positions were outliers more than 20 times, and thus represented the bulk of the outliers. A quick examination of several of these does not show anything obvious that would account for this behavior, though we do not rule out the possibility of elevated noise in the simulated image due to noisy hot, unstable, or sink pixels in the dark calibration reference file. Given the small difference in measured and intrinsic polarization fraction, we focus our discussion on systematics observed in our data rather than effects due to random errors. We do note that the small values of $P - P_0$ indicate that the effects of the CTE correction on ACS/WFC polarimetry accuracy are negligible compared to other sources of uncertainty that observers are likely to encounter, e.g., instrumental polarization (diattenuation, phase retardation, and polarization effects from the tilt of the WFC CCDs), uncertainty in the polarizer throughputs, and accuracy of the reference calibration files. See Biretta et al. (2004) for more information.

3.1 Polarization Fraction

As previously discussed, one of the most important factors contributing to CTE loss is the number of y -transfers between a pixel and the serial register. Figure 2 shows, for the CTE-corrected FLC data, the difference between the measured polarization fraction P and intrinsic polarization fraction P_0 as a function of the number of y -transfers to the serial register. We find that the difference $P - P_0$ increases with the number of y -transfers, and therefore with worsening CTE loss. We additionally find that $P - P_0$ exhibits a strong systematic increase with increasing polarization fraction. Interestingly, we do not find a strong dependence on the source magnitude (see below), though this is likely due to the CTE correction performing well over a much larger range of source brightness compared to our grid, which was limited to brightnesses suitable for ACS polarimetry.

In Figure 3, we again show the difference $P - P_0$ as a function of y -transfers, but this time for the non-CTE-corrected FLT data. Compared to Figure 2, we immediately observe

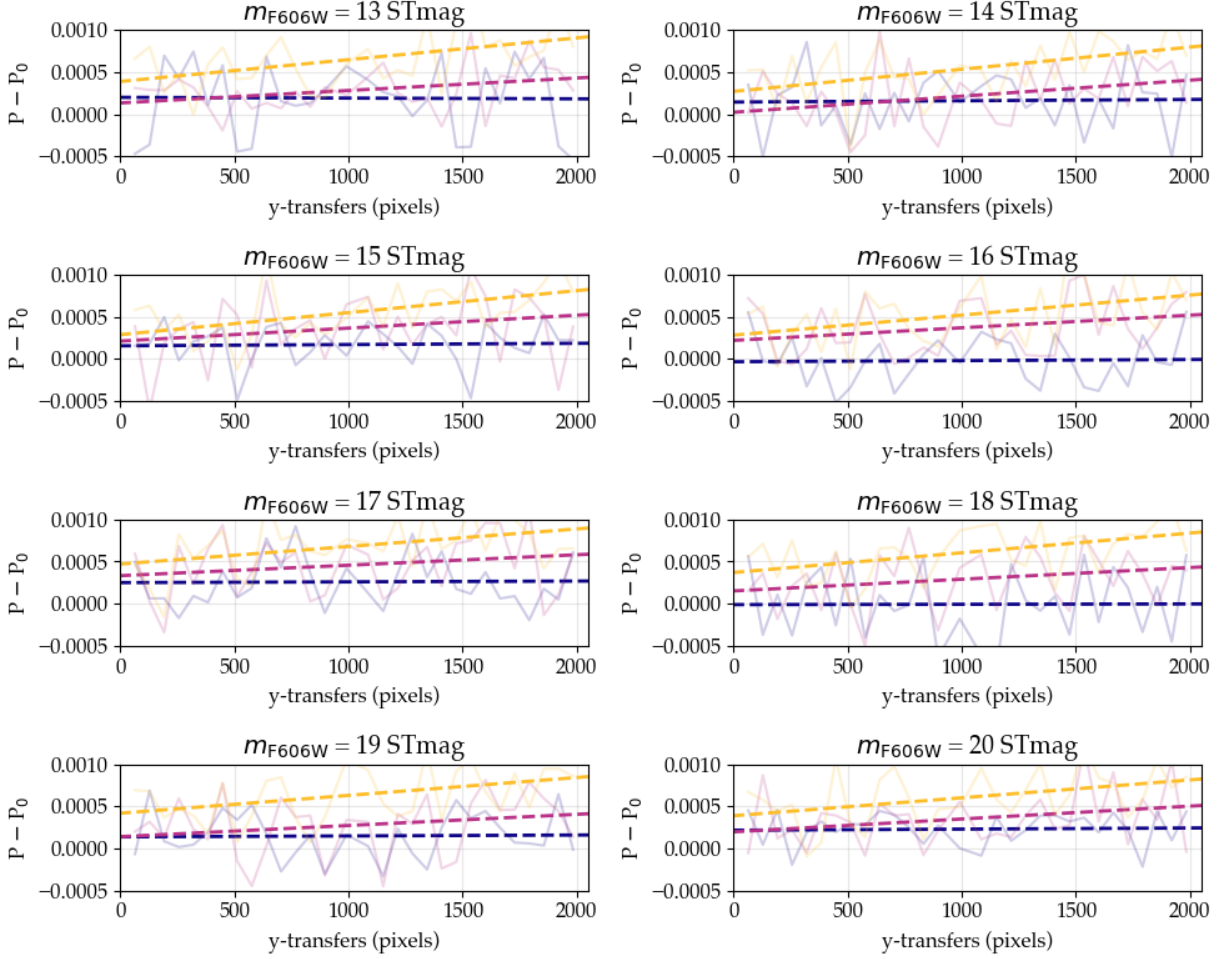


Figure 2: Difference between the polarization fraction P measured from CTE-corrected (FLC) images and the intrinsic polarization fraction P_0 as a function of the number of y -transfers to reach the serial register. To aid in visibility, we only plot the $P_0 = [0.05, 0.5, 1.0]$ data (blue, pink, and yellow, respectively). Transparent, solid lines represent the mean difference for each row of stars in the simulated images, while dashed lines show the linear fit to the unbinned data. Each panel is labeled with the associated point source brightness in magnitudes, and the axis scales are the same in each panel. At each magnitude, the higher polarization data show a steeper offset in $P - P_0$ as a function of y -transfers.

that the positive correlation between $P - P_0$ and y -transfers in the FLC data has changed to either no correlation or a weak negative correlation. The slightly negative correlation is most likely due to increasing CTE loss with additional y -transfers to reach the serial register, which causes an increasing amount of charge to trail out of the source. We do not expect $P - P_0 > 0$ at few y -transfers in the FLT data where there should be little-to-no CTE loss. Low polarization sources (the blue $P = 0.05$ line in the figure) show no correlation between $P - P_0$ and y -transfers, while the intermediate polarization (the pink $P = 0.5$ line) sometimes has $P - P_0 > 0$ at few y -transfers, and the $P = 1.0$ data always exhibit some positive offset. We suspect that this offset at $y = 0$ is not real, and is possibly due to a small systematic error introduced by the CTE forward model when simulating the FLT data. The FLC data are simulated by CTE-correcting the FLT data, therefore some small residual offset is likely

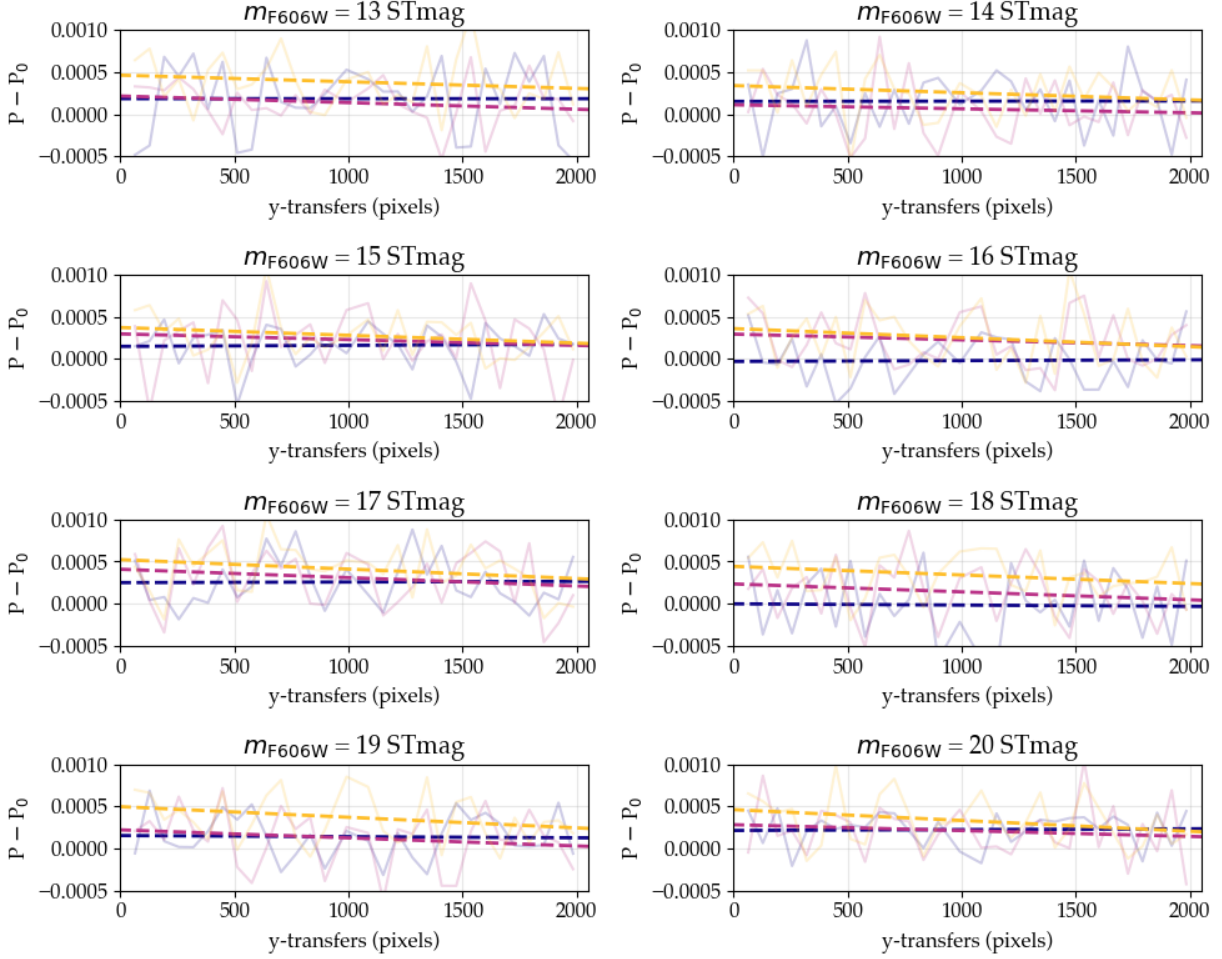


Figure 3: Similar to Figure 2, here we show the difference between the polarization fraction P measured from non-CTE-corrected (FLT) images and the intrinsic polarization fraction P_0 as a function of the number of y -transfers to reach the serial register. The colors, line styles, and axis scales are the same as in Figure 2. We find either no correlation or a slightly negative correlation between $P - P_0$ with increasing y -transfers likely due to CTE loss. The small offset in $P - P_0$ near $y = 0$ is likely indicative of a small systematic effect in our simulated data.

also present in Figure 2, and indeed the offsets in the FLC data at $y = 0$ are similar in size compared to the FLT data. Despite this small systematic offset at $y = 0$, we do not think it has much effect on the slopes of the FLC data fits, and has only maybe slightly increased the fit intercept. We note that the FLT exhibit a smaller offset across all values of y -transfers. This is likely due to the use of a large photometric aperture with an isolated point source wherein we are capturing most of the charge in the CTE trail within the aperture. Such a scenario may or may not be applicable to real observations due to, e.g., source crowding.

In Figures 4 and 5, we show the percentage difference of the measured Stokes I , Stokes U , and polarization fraction P values compared to the intrinsic values as a function of the number of y -transfers for the FLC and FLT data, respectively. In these figures, we show only 100% polarized sources with $m_{F606W} = 13$ STmag and row-averaged on the CCDs. Sources with lower polarization and/or fainter magnitudes show identical behavior with

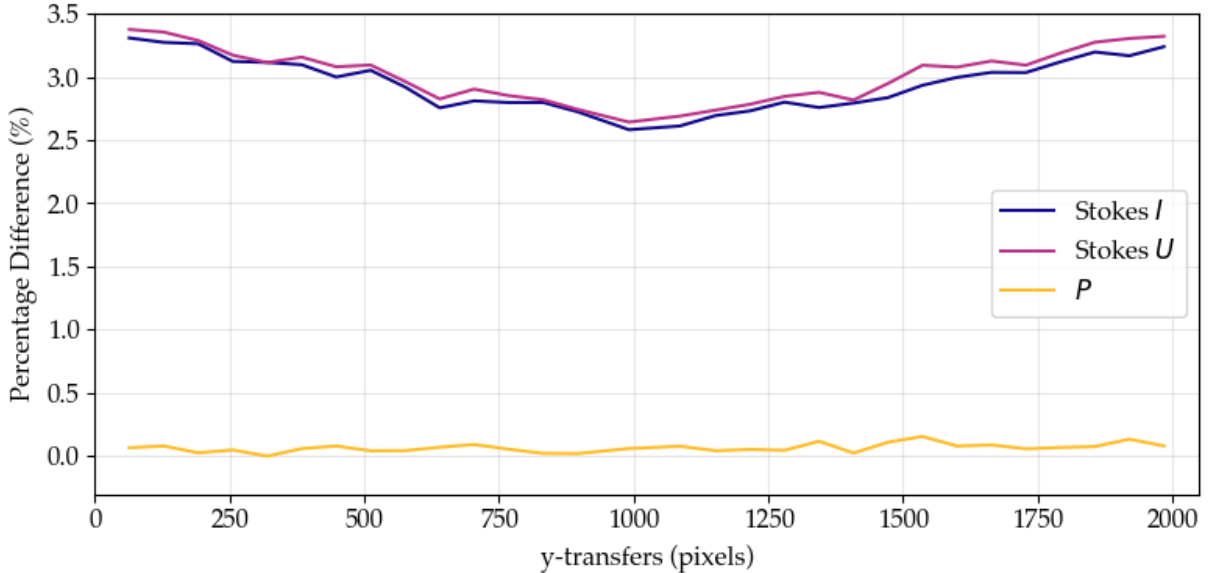


Figure 4: Here we show the percentage difference of the Stokes I , Stokes U , and polarization fraction (P) values measured from the CTE-corrected FLC data compared to their intrinsic values as a function of the number of y -transfers for 100% polarized sources with $m_{F606W} = 13$ STmag. We observe a strong, parabolic feature in the Stokes parameters with the inflection point near the center of the CCDs. Conversely, the polarization fraction follows a more linear trend with increasing y -transfers with a much smaller offset from the intrinsic polarization fraction (see Figure 2) The difference in the shape of the Stokes parameters compared to the polarization fraction is due to the calculation of the polarization fraction being the ratio of the Stokes values.

increased noise, therefore we only show these data as an illustrative example. In the FLC data (Figure 4), we observe a parabolic distribution in the percentage difference of the Stokes parameters as a function of the y -transfers. The inflection point of the distribution is near the center of the WFC CCDs, which may be a result of the complex effects of the CTE correction the calculation of the Stokes parameters, which are themselves linear combinations of photometric measurements (see Section 2.1). Whatever the cause, the effect in the FLC data is small ($< 1\%$ peak-to-peak), and represents a significant improvement over the distribution observed in the FLT data (Figure 5; a change of approximately 3.5% across the CCDs). The similar values of the Stokes I and U percentage differences at $y = 0$ in both the FLC and FLT data helps to affirm our hypothesis that there is a small systemic effect present in our simulated data. As previously discussed, this effect likely only impacts the absolute offsets of our measurements compared to the intrinsic polarization properties of our simulated data, and not our ability to examine systematic trends such as the increase in $P - P_0$ as a function of polarization fraction. Despite the larger change in Stokes parameters as a function of y -transfers in the FLT data, the values of Stokes I and U track much closer together compared to the FLC data resulting in a slightly more accurate estimate of the polarization fraction as a function of y -transfers from non-CTE-corrected images (see also Figures 2 and 3).

Tables 1 and 2 give the fit parameters for $P - P_0$ as a function of y -transfers for the FLC

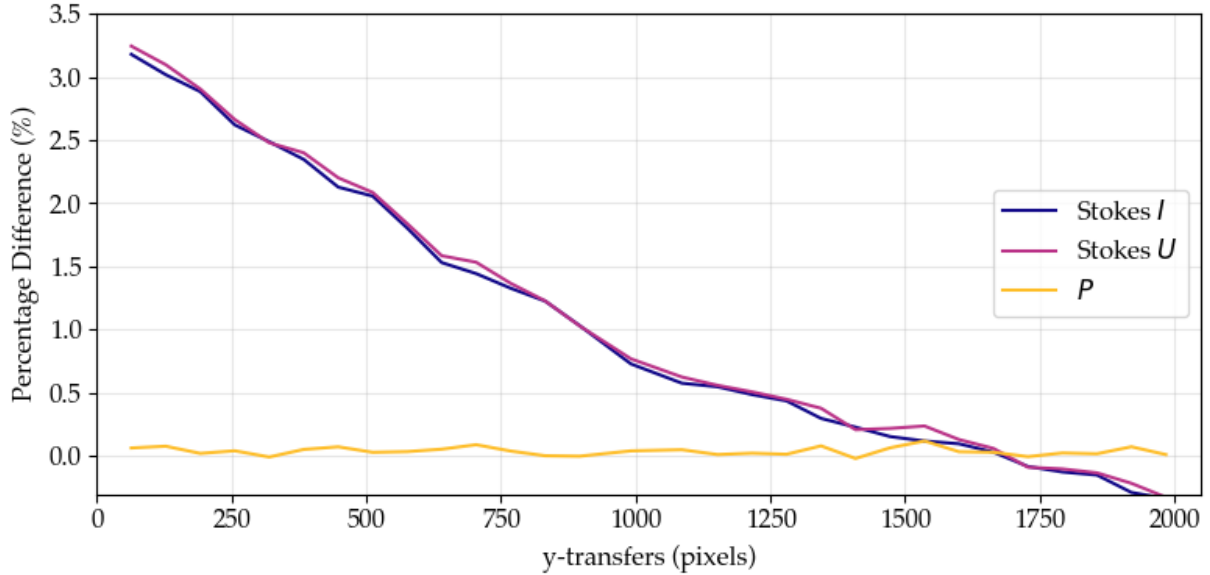


Figure 5: Similar to Figure 4, here we display the same information, but for the non-CTE-corrected FLT data. Instead of a parabolic feature in the Stokes parameters, we observe a strongly negative correlation with increasing y -transfers. The percentage difference of the Stokes parameters at $y = 0$ is similar in both the FLT and FLC data, which corroborates the hypothesis that this is a systematic effect in our simulated data. The negative correlation between the Stokes parameters and number of y -transfers is likely the result of increasing CTE loss.

and FLT data, respectively, i.e.:

$$(P - P_0) = ay + y_0,$$

where a is the slope, y is the number of y -transfers, and y_0 is the intercept. We use this information to plot the slopes (grouped by P_0) as a function source magnitude for the FLC data in Figure 6. Similar to our initial findings from Figure 2, we find that the slope of the offset $P - P_0$ as a function of y -transfers clearly increases with increasing polarization fraction. We attribute this polarization dependence on the unequal distribution of signal in the three polarization filters (see the Stokes equations in Section 2.1). Examining the slopes as a function of source magnitude in Figure 6 shows no correlation, again likely due to the CTE correction performing well across this magnitude range. Note that while the values of the slopes span an order of magnitude for the full range of polarization fractions, these slopes are all extremely small ($\sim 10^{-7}$).

3.2 Polarization Position Angle

Similar to Figure 2, in Figure 7 we show the difference $|\theta - \theta_0|$ as a function of y -transfers for a subset of the simulated FLC data with polarization fractions $P_0 = [0.05, 0.5, 1.0]$. Recall from Section 2 that the uncertainty in the measured position angle of the electric field vector θ from Sparks & Axon (1999) varies considerably more than the polarization fraction uncertainty. For our simulated grid parameters, we expect $0.069 \leq \sigma_\theta \leq 4.5^\circ$ for $P_0 = 1.0$

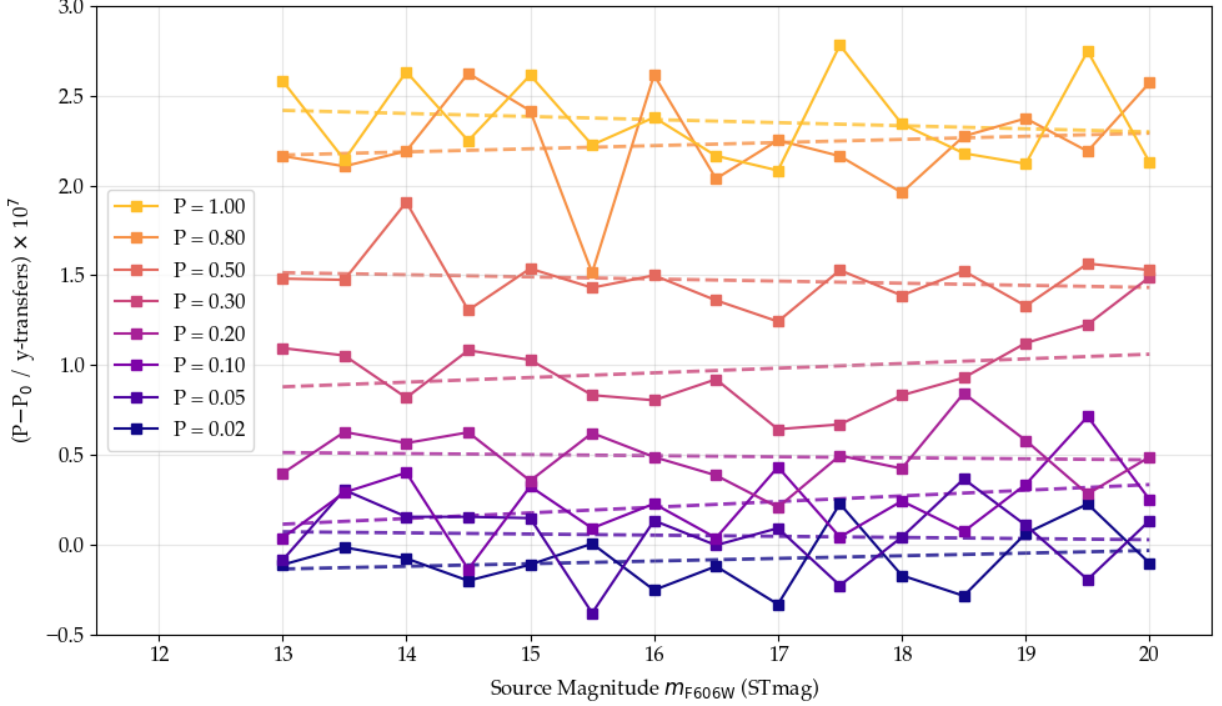


Figure 6: The slope of the offset $P - P_0$ measured from the FLC data as a function of the number of y -transfers from Figure 2 plotted against the simulated source magnitude. The slopes for different values of P_0 are shown in different colors. Squares connected by solid lines show the slope values, while dashed lines represent a linear fit to the slopes as a function of source magnitude. The slope of $P - P_0$ as a function of y -transfers very clearly increases with increasing polarization fraction; however, no dependence is observed with source magnitude.

and 0.02, respectively, with $S/N = 260$. From Figure 7, we find no systematic relationship between the offset $|\theta - \theta_0|$ with increasing number of y -transfers. This result is somewhat artificial as Stokes Q asymptotically approaches zero at $\theta = 45^\circ$, thus smoothing out much of the variation we measure in Stokes U . We do observe that the data with the lowest polarization in the figure ($P = 0.05$) exhibit the largest offset ($|\theta - \theta_0| \approx 1.5^\circ$) in position angle, though it is within the expected random uncertainty $\sigma_\theta = 1.67^\circ$ for that polarization fraction. For completeness, we include $|\theta - \theta_0|$ as a function of y -transfers measured from the FLT data in Figure 8.

4 Conclusion

We report on the accuracy of the polarization properties measured from simulated ACS/WFC images that have been corrected for CTE loss using the pixel-based CTE correction in the ACS data pipeline. Despite evidence of an offset present in our simulated ACS observations, we find systematic effects due to the pixel-based CTE correction that lead to a small overestimation of the polarization fraction ($P - P_0 \leq 0.01$) of point sources. This overestimation in polarization fraction is positively correlated with:

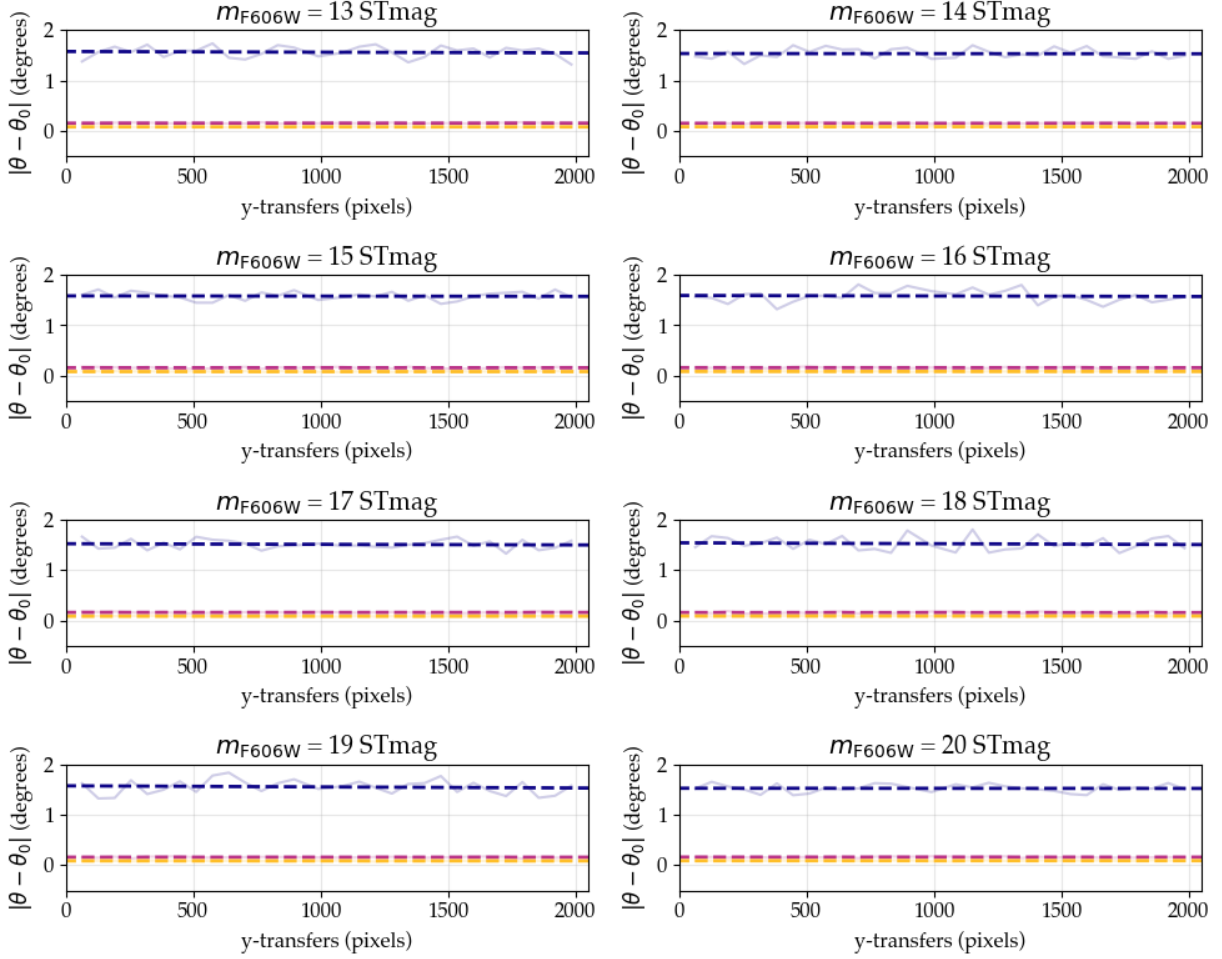


Figure 7: Similar to Figure 2, here we show the difference between the electric field vector position angle θ measured from CTE-corrected (FLC) images and the intrinsic position angle θ_0 as a function of the number of y -transfers to reach the serial register. The colors and line styles are the same as in Figure 2. No dependence is observed between $|\theta - \theta_0|$ and the number of y -transfers.

1. the number of y -transfers between the source and the serial register, and
2. the polarization fraction of the source.

Over the range of source magnitudes that are useful for ACS polarimetry, we find no correlation with source brightness. We stress that these systematic overestimations we find are negligible compared to other sources of uncertainty that dominate ACS polarimetry data. Unlike the polarization fraction, we find that the Stokes parameters measured across the WFC CCDs are much better behaved in a relative sense in the CTE-corrected data ($\leq 1\%$ percentage difference peak-to-peak) compared with the non-CTE-corrected data ($\approx 3.5\%$ percentage difference decline across the WFC CCDs). We also examine the impact of the CTE correction on the measurement of the electric field vector position angle, but find no systematic effects.

These results should serve to assure ACS users of the fidelity of polarization data that

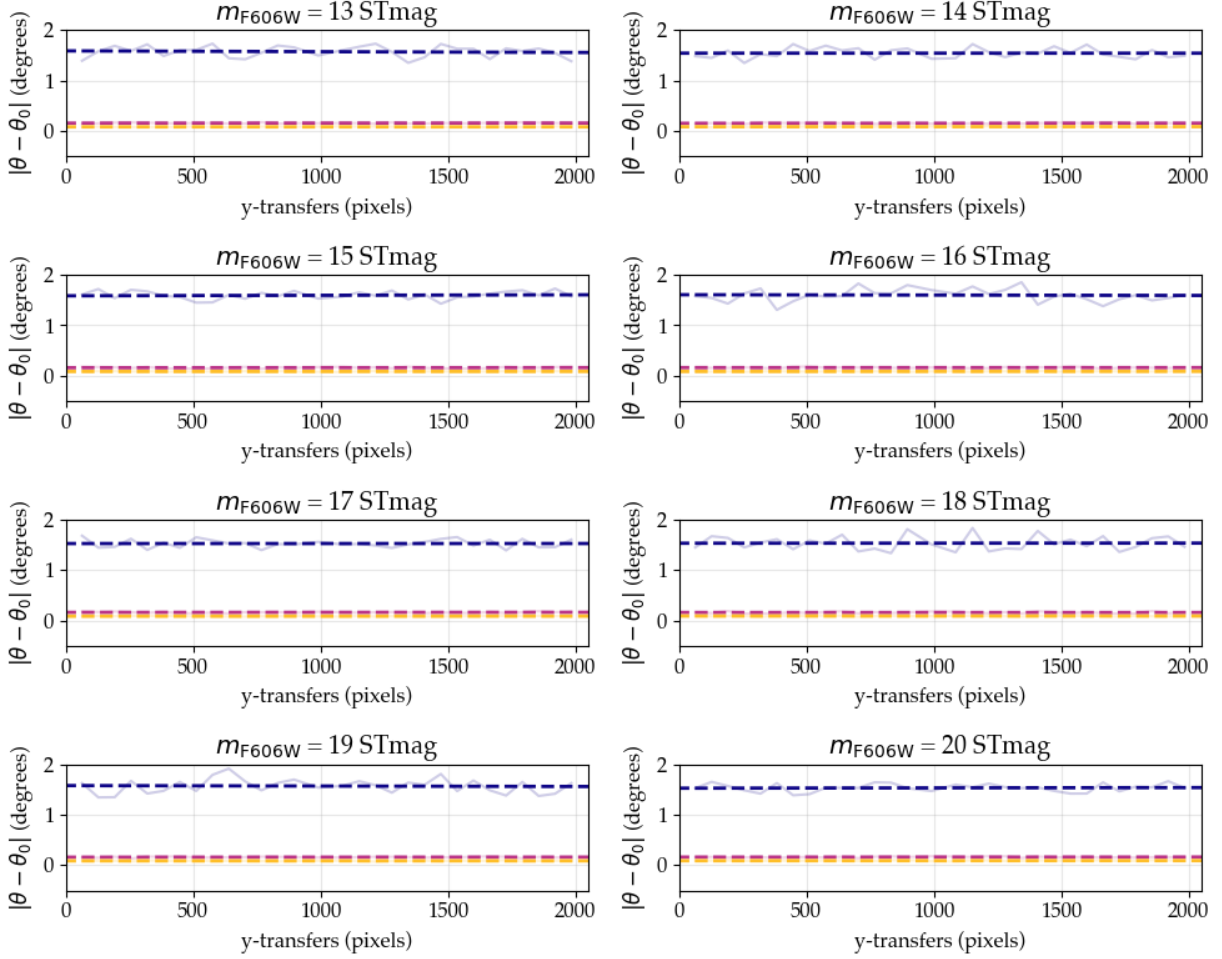


Figure 8: As in Figure 7, here we show the difference between the electric field vector position angle θ measured from non-CTE-corrected (FLT) images and the intrinsic position angle θ_0 as a function of the number of y -transfers to reach the serial register. The colors and line styles are the same as in Figure 2. The plots are almost identical to those in Figure 7 showing no dependence between $|\theta - \theta_0|$ and the number of y -transfers.

have been processed using the pixel-based CTE correction. The simulated data used in this study are reasonably representative of real observations with the ACS/WFC, however real observations may have additional effects not included here (e.g., cosmic rays), or suffer from non-ideal signal-to-noise or source crowding. Furthermore, different polarization position angles may result in more complex distributions of count rates in the three polarization filters, which may impact the degree to which the CTE correction affects the calculation of the Stokes parameters and polarization properties. We find that using FLT data with a large ($r = 10$ pixels) photometric aperture better recovers the intrinsic polarization fraction, but that the FLC data provide a more stable measurement of the Stokes parameters across the CCDs. Given that the offset in the polarization fraction measured from the FLC data is small, we advise that users perform polarimetry analysis on FLC data when possible, particularly for situations in which CTE loss is significant.

We note that the scope of our analysis is limited to the effect of the CTE correction on point sources for a single polarization angle. A more complex analysis is required to assess the impact of the CTE correction on the accuracy of ACS polarimetry measurements for a range of source parameters that may impact the CTE correction in other ways (e.g., varying polarization angles), and for extended sources, for which the pixel-based CTE correction is necessary.

Acknowledgements

This research made use of Photutils, an Astropy package for detection and photometry of astronomical sources (Bradley et al., 2020). The authors are grateful to Jenna Ryon, Nimish Hathi, Samantha Hoffmann, and Ralph Bohlin for their helpful comments in the preparation of this manuscript.

References

- Anderson, J., & Bedin, L. 2010, An Empirical Pixel-Based Correction for Imperfect CTE. I. HST's Advanced Camera for Surveys, Instrument Science Report ACS 2010-03
- Anderson, J., & Ryon, J. E. 2018, Improving the Pixel-Based CTE-correction Model for ACS/WFC, Instrument Science Report ACS 2018-04
- Bellini, A., Anderson, J., & Grogin, N. A. 2018, Focus-diverse, empirical PSF models for the ACS/WFC, Technical Instrument Report ACS 2018-08
- Biretta, J., et al. 2004, ACS Polarization Calibration - I. Introduction and Status Report, Instrument Science Report ACS 2004-09
- Bradley, L., Sipőcz, B., Robitaille, T., et al. 2020, astropy/photutils: 1.0.0, doi:10.5281/zenodo.4044744
- Chiaberge, M. 2012, A New Accurate CTE Photometric Correction Formula for ACS/WFC, Instrument Science Report ACS 2012-05
- Chiaberge, M., Lim, P. L., Kozhurina-Platais, V., Sirianni, M., & Mack, J. 2009, Updated CTE Photometric Correction for WFC and HRC, Instrument Science Report ACS 2009-01
- Lucas, R. A., et al. 2021, ACS Data Handbook, Version 10.0
- Riess, A. 2003, On-Orbit Calibration of ACS CTE Corrections for Photometry, Instrument Science Report ACS 2003-09
- Riess, A., & Mack, J. 2004, Time Dependence of ACS WFC CTE Corrections for Photometry and Future Predictions, Instrument Science Report ACS 2004-006
- Ryon, J. E., & Grogin, N. A. 2018, ACS/WFC Parallel CTE from EPER Tests, Instrument Science Report ACS 2018-09

Ryon, J. E., et al. 2021, ACS Instrument Handbook, Version 20.0

Sparks, W. B., & Axon, D. J. 1999, Publications of the Astronomical Society of the Pacific, 111, 1298

STScI Development Team. 2013, pysynphot: Synthetic photometry software package, ascl:1303.023

Ubeda, L., Anderson, J., & ACS Team. 2012, in American Astronomical Society Meeting Abstracts, Vol. 219, American Astronomical Society Meeting Abstracts #219, 241.03

Table 1: Fit Parameters for $P - P_0$ as a Function of y -transfers for FLC Data

m_{F606W}	Slopes ($10^7 a$)										Intercepts ($10^4 y_0$)									
	$a_{0.02}$	$a_{0.05}$	$a_{0.10}$	$a_{0.20}$	$a_{0.30}$	$a_{0.50}$	$a_{0.80}$	$a_{1.00}$	$y_{0,0.02}$	$y_{0,0.05}$	$y_{0,0.10}$	$y_{0,0.20}$	$y_{0,0.30}$	$y_{0,0.50}$	$y_{0,0.80}$	$y_{0,1.00}$				
13.0	-0.11	-0.09	0.04	0.40	1.09	1.48	2.16	2.58	3.31	2.01	-0.05	1.75	2.73	1.35	2.16	3.91				
13.5	-0.02	0.30	0.29	0.63	1.05	1.47	2.11	2.14	2.09	1.23	1.91	1.25	2.03	2.34	3.09	3.90				
14.0	-0.08	0.15	0.40	0.57	0.82	1.91	2.19	2.63	2.67	1.45	0.90	-0.19	1.11	0.24	2.74	2.72				
14.5	-0.20	0.15	-0.14	0.62	1.08	1.31	2.63	2.25	2.20	2.34	1.83	-0.17	1.67	1.32	1.89	3.42				
15.0	-0.11	0.15	0.32	0.36	1.03	1.54	2.42	2.61	3.33	1.57	1.51	-0.02	1.93	2.13	1.73	2.89				
15.5	0.00	-0.38	0.09	0.62	0.83	1.43	1.51	2.23	2.81	2.36	0.79	1.56	2.02	0.94	3.62	2.97				
16.0	-0.25	0.13	0.23	0.49	0.80	1.50	2.62	2.38	4.56	-0.33	1.54	1.17	1.88	2.21	2.35	2.84				
16.5	-0.12	0.00	0.04	0.39	0.92	1.36	2.04	2.17	2.97	2.03	1.89	0.77	1.72	1.97	2.58	3.53				
17.0	-0.33	0.09	0.43	0.21	0.64	1.24	2.25	2.08	2.78	2.50	0.79	0.37	1.82	3.33	2.68	4.71				
17.5	0.23	-0.23	0.04	0.50	0.67	1.53	2.16	2.78	3.13	0.97	2.29	0.56	2.68	1.81	2.53	1.63				
18.0	-0.17	0.04	0.24	0.42	0.83	1.39	1.96	2.34	2.88	-0.11	0.43	1.54	1.74	1.52	3.10	3.70				
18.5	-0.29	0.37	0.07	0.84	0.93	1.52	2.27	2.18	2.16	2.23	0.60	-0.01	3.04	2.36	3.41	3.50				
19.0	0.06	0.11	0.33	0.58	1.12	1.33	2.37	2.12	1.59	1.37	1.74	2.40	1.04	1.39	3.02	4.18				
19.5	0.23	-0.20	0.71	0.28	1.23	1.57	2.19	2.75	3.31	2.56	0.97	1.55	0.75	1.15	2.16	3.19				
20.0	-0.10	0.13	0.25	0.49	1.49	1.53	2.57	2.13	0.73	2.15	1.30	0.48	1.20	1.96	2.01	3.88				

Table 2: Fit Parameters for $P - P_0$ as a Function of y -transfers for FLT Data

m_{F606W}	Slopes ($10^7 a$)										Intercepts ($10^4 y_0$)									
	$a_{0.02}$	$a_{0.05}$	$a_{0.10}$	$a_{0.20}$	$a_{0.30}$	$a_{0.50}$	$a_{0.80}$	$a_{1.00}$	$y_{0,0.02}$	$y_{0,0.05}$	$y_{0,0.10}$	$y_{0,0.20}$	$y_{0,0.30}$	$y_{0,0.50}$	$y_{0,0.80}$	$y_{0,1.00}$				
13.0	-0.18	0.00	-0.64	-0.71	-0.36	-0.79	-0.48	-0.79	3.14	1.86	0.09	2.18	3.35	2.17	3.32	4.65				
13.5	-0.16	0.11	-0.52	-0.32	-0.46	-0.85	-0.68	-1.11	2.08	1.39	2.13	1.63	2.64	3.28	4.38	4.60				
14.0	-0.10	0.03	-0.38	-0.56	-0.68	-0.47	-0.25	-0.85	2.70	1.53	1.12	0.30	1.75	1.13	3.77	3.41				
14.5	-0.34	0.05	-0.84	-0.33	-0.36	-0.86	0.27	-1.12	2.32	2.27	2.03	0.20	2.25	2.26	2.85	4.05				
15.0	-0.47	0.12	-0.36	-0.56	-0.25	-0.68	-0.05	-0.93	3.63	1.50	1.79	0.29	2.41	2.98	2.73	3.74				
15.5	-0.26	-0.42	-0.75	-0.26	-0.66	-0.83	-0.92	-1.34	3.02	2.38	1.00	1.86	2.72	1.74	4.75	3.94				
16.0	-0.26	0.10	-0.55	-0.64	-0.87	-0.69	0.09	-1.08	4.39	-0.29	1.72	1.69	2.70	2.95	3.39	3.61				
16.5	-0.13	-0.36	-0.69	-0.57	-0.69	-0.83	-0.47	-1.35	2.78	2.27	1.94	1.08	2.47	2.85	3.68	4.30				
17.0	-0.44	0.07	-0.51	-0.84	-0.81	-0.99	-0.38	-1.12	2.79	2.50	1.09	0.78	2.34	4.09	3.93	5.23				
17.5	0.10	-0.39	-0.77	-0.50	-0.73	-0.82	-0.50	-0.85	3.08	1.10	2.57	0.97	3.33	2.70	3.65	2.49				
18.0	-0.35	-0.15	-0.50	-0.67	-0.39	-0.94	-0.57	-1.02	3.05	-0.02	0.58	2.13	2.16	2.35	4.20	4.43				
18.5	-0.41	-0.03	-0.74	-0.18	-0.44	-0.68	-0.08	-1.48	2.21	2.58	0.84	0.45	3.49	3.25	4.36	4.50				
19.0	0.00	-0.13	-0.46	-0.40	-0.19	-0.95	-0.14	-1.26	1.46	1.52	1.97	2.79	1.54	2.20	3.85	4.96				
19.5	0.16	-0.19	-0.34	-0.65	-0.41	-0.85	-0.44	-0.72	3.27	2.49	1.35	1.86	1.61	2.13	3.20	4.06				
20.0	-0.17	0.10	-0.67	-0.62	0.11	-0.69	-0.10	-1.29	0.68	2.13	1.56	1.10	1.66	2.81	3.18	4.60				